Solid Freeform Fabrication 2019: Proceedings of the 30th Annual International
Solid Freeform Fabrication Symposium – An Additive Manufacturing Conference
Reviewed Paper

Effect of Preheating Build Platform on Microstructure and Mechanical Properties of Additively Manufactured 316L Stainless Steel

P.D. Nezhadfar[1,2], Arash Soltani-Tehrani[1,2], Nima Shamsaei[1,2]

[1] Department of Mechanical Engineering, Auburn University, Auburn, AL 36849, USA
[2] National Center for Additive Manufacturing Excellence (NCAME), Auburn University, Auburn, AL 36849, USA

Abstract

This study aims to understand the effect of build platform preheating on the microstructural features and mechanical properties of 316L stainless steel (SS) fabricated via laser beam powder bed fusion (LB-PBF) process. Two sets of specimens were fabricated on a non-preheated build platform and the build platform preheated to 150 °C. Thermal simulations are carried out using ANSYS using additive manufacturing module to investigate the variation in thermal history experienced by the specimens in each condition. Microstructural features are analyzed via simulation, and the results are validated experimentally. In addition, the effect of preheating on the porosity size and distribution is evaluated using digital optical microscopy. Mechanical properties of specimens from each condition are further assessed and correlated to the variations in microstructure and defect size distributions.

Keywords: Laser beam powder bed fusion (LB-PBF); Preheating; Stainless steel; Porosity; Mechanical properties; Microstructure

Introduction

Establishing process-structure-property-performance (PSPP) relationships for various material systems fabricated via additive manufacturing (AM) techniques has been becoming of particular interest for various industrial sectors. Although AM provides an opportunity to manufacture parts with complex geometries, the intricate thermal history experienced by the parts during fabrication leads to the formation of defects (i.e. pores, lack of fusion, surface roughness), producing anisotropic microstructure [1,2] as well as inducing residual stress. Daniewicz and Shamsaei [1] introduced the fatigue and fracture of additively manufactured parts as the most challenging issue hindering the adoption of AM for critical load bearing components. Several other studies also have shown that the presence of the aforementioned defects reduces the fatigue resistance of AM parts. Accordingly, as the most critical load-bearing parts are usually experiencing cyclic loading in service, it is essential to reduce defects and microstructure heterogeneity by controlling the thermal history.

Thermal history is controlled by the employed process parameters (i.e. laser power, scan speed, scan strategy, etc.) [3], part size and geometry [4], build orientation [5], and the fabrication environment (due to shielding gas thermal properties and enclosure walls) [6]. These have been reported as the controlling parameters for reducing the defects and anisotropy in the microstructure [2] and residual stress. Moreover, controlling thermal history may eliminate the need for post-processing procedures (e.g. heat treatment, surface machining, hot isostatic pressing (HIP)), which expedites the adoption of AM for widespread industrial applications and reduces the cost of such procedures.

Shrestha et al. [4] studied the effect of part size and geometry on the thermal history and mechanical properties of laser beam powder bed fusion (LB-PBF) 17-4 PH stainless steel (SS). They showed that small changes in the size and geometry of the part will change the thermal history experienced by the part, thereby influencing the defect size and distribution. They also reported better fatigue resistance for specimens machined out from square bars as compared to the ones fabricated slightly oversized than the near net-shape. This was attributed to the higher bulk temperature in former specimens and led to the formation of lower porosity level.

Gu et al. [7] studied the effects of energy density on the microstructure and porosity formation in LB-PBF 17-4 PH SS by altering the scan speed and laser power. Results showed that lower porosity level will be achieved by adjusting the energy density in the range of 44-81 J/mm^3. However, they showed that energy density cannot be a good indication of the porosity level. For instance, increased scan speed and laser power led to the lower energy density in the range, however, the porosity level increased due to the balling phenomenon. Sun et al. [8] produced a unique crystallographic lamellar microstructure (CLM) in LB-PBF 316L SS via controlling the energy density. The newly developed texture for this material comprised of two grain orientations, <001> and <011>, which enhanced the mechanical properties significantly.

Thermal history was also observed to be sensitive to the build platform temperature during fabrication through AM process. It was reported that preheating the build platform can lead to lower residual stress, more homogenized microstructure, and consequently, better mechanical properties (e.g. ductility, fatigue resistance, and etc.) as compared to the condition without preheating the build platform [9]. Yang et al. [10] investigated the effect of preheating the build platform at constant energy densities on the microstructure of Al-Mg (-Sc)-Zr. They observed columnar to equiaxed grain morphology as the build platform preheated at 200 °C. They attributed this microstructure evolution to the reduced thermal gradients and increased remelting zone volumes. Liu et al. [11] investigated the effects of various build platform preheating temperatures on the texture evolution of TiAl alloy via LB-PBF process. They reported significant differences between the grain orientations obtained under different preheating temperatures.

Accordingly, due to the complexity of changing process parameters such as laser power, scan speed, scan strategy, etc., fabricating parts by preheating the build platform can be a solution to manufacture parts with more homogeneous microstructure and less residual stress. Austenitic stainless steel 316L is one of the most attractive materials in various industrial sectors. Moreover, its biocompatibility and corrosion resistance make this material suitable for medical applications such as bone implants [12]. The goal of this study is to investigate the effects of build platform preheating on the microstructure and porosity level of LB-PBF 316L SS. Numerical simulations are carried out using ANSYS Additive Manufacturing module to calculate the variation in cooling rates. Numerical simulations are then validated by experimental observations of the melt pool dimensions and microstructural variation for different cooling rates. Eventually, the porosity size and distribution are evaluated for specimens fabricated with preheating the build plate and compared with the ones fabricated without preheating the build plate. Tensile deformation behavior is assessed for each condition and correlated to the microstructure and porosity size and distribution.

Experimental Procedures

In this study, 316L stainless steel (SS) powder provided by LPW Inc. with the chemical composition listed in Table 1 was used to fabricate specimens. The specimens were fabricated via a laser beam powder bed fusion (LB-PBF) method in the vertical direction using Renishaw AM 250 machine.

Table 1. Chemical composition of 316L SS powder, provided by LPW Technology Inc.

	Cr	Ni	Mn	Si	Nb	Mo	N	O	P	S	Fe
(Wt. %)	16-18	4.03	0.20	0.10	0.33	2.0-3.0	<0.10	<0.10	<0.04	<0.03	Bal.

Two sets of specimens were fabricated under argon shielding gas, without and with preheating the build platform to 150°C. Specimen geometry is shown in Figure 1. For better tracking each set of specimens in the following context, specimens fabricated without preheating the build platform, and the ones fabricated with preheating the build platform to 150 °C are designated by NP and P150, respectively.

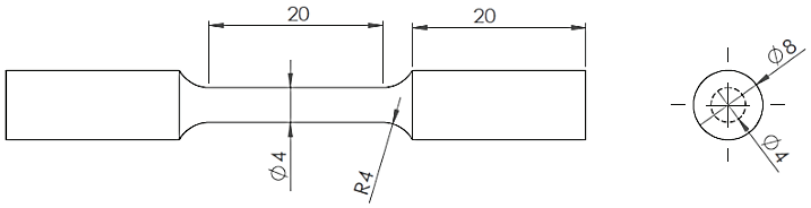

Figure 1. Drawing of sub-sized tensile specimens based on the ASTM E8 standard.

Thermal properties were predicted for each condition (i.e. NP and P150) employing the commercial ANSYS Additive Manufacturing module. In this module, deposition thickness, scan speed, hatch spacing, layer time interval, preheating temperature, and powder and gas convection coefficients were input to the software. Software input parameters were selected based on the manufacturing machine (i.e. Renishaw AM 250) and optimized process parameters for 316L SS (i.e. layer thickness of 50 μm, hatch spacing of 0.11 mm, laser power of 200 W, and a scan speed of 1833 mm/s). The layer time interval in the gauge section was 65 s recorded during the fabrication process. Material (i.e. 316L SS) was selected from the ANSYS database with pre-defined temperature-dependent properties including density, thermal conductivity, and heat capacity. Computer-aided designed (CAD) or stereolithography (STL) files of fabricated specimens were imported directly to ANSYS to perform the numerical analyses. In addition, the build platform was considered in the design in order to consider the heat dissipation to the build plate. The software outputs were the maximum and minimum temperatures in each layer depending on the fabrication time. In ANSYS Additive Manufacturing module, temperatures are obtained by solving the partial differential equation (PDE) of conduction heat transfer given in Eq. 1, which is the main source of heat dissipation in LB-PBF process given [13].

$$\rho c \frac{\partial T}{\partial t} = \frac{\partial}{\partial x}\left(k \frac{\partial T}{\partial x}\right) + \frac{\partial}{\partial y}\left(k \frac{\partial T}{\partial x}\right) + \frac{\partial}{\partial y}\left(k \frac{\partial T}{\partial x}\right) + \dot{q} \quad \text{Eq. 1}$$

In which, T is the temperature as a function of time and location. The ρ, k, and c are material temperature-dependent density, thermal conductivity, and heat capacity, respectively. In addition, $\dot{q}$ is the heat input per volume due to laser beam source, which is considered via a Gaussian distribution [13]. Convection and radiation heat losses can be also considered as the boundary conditions to solve the PDE [13]. However, in this study, the effects of convection and radiation were neglected to simplify the model. Finally, specimen drawings were cut in the middle of the gauge and used for numerical analyses in order to focus on the thermal history of the gauge section as well as decreasing the processing time. The heat transfer coefficients of powder and shielding gas (i.e. argon) were selected as a relatively small number to ensure that conduction is the main source of heat dissipation. Two simulations were performed based on the two experiments, one with preheating the build platform of 150 °C and one without preheating. In addition, the mesh size was selected as 0.2 mm to ensure the mesh discrepancy of the results. The build plate was meshed with an element size of 5 mm since it was kept at a constant temperature during the fabrication time.

For microstructure characterization, some specimens were fabricated to the half-height of the regular ones. Those specimens were transversely cut perpendicular to the final laser tracks to look into the melt pool's geometry. Microstructure samples were then ground using 320-2500 grit sandpapers to the mirror-like surface finish. Prior to reveal the microstructure, porosity measurement was carried out using KEYENCE digital optical microscope. Specimens were further etched to reveal the microstructure, showing the grains and melt pool dimensions on the most top fabricated layer.

Tensile tests at 0.001 s^{-1} strain rate were conducted at room temperature using an MTS Landmark servohydraulic test system with 100 kN load cells. Tests were conducted in two steps, strain-controlled mode followed by displacement-control mode. Strain-control mode step was performed up to 0.045 strain using an MTS extensometer to record the strain. However, due to the limited displacement of extensometer and to avoid any damage, tests were paused to remove the extensometer. Subsequently, tests were continued in displacement-controlled mode to fracture with a velocity equivalent to the same strain rate. To obtain the elongation to failure, gage sections were marked prior testing, and measured after tests were done. Two tests were conducted for each condition to observe the consistency of the results. To understand the fracture behavior in each condition, fractography analysis was carried out for all the tested specimens using KEYENCE digital microscope.

Results and Discussion

Thermal Simulation and Microstructure

Figure 2 shows a time window of the interlayer temperature fluctuation during fabrication for each condition (i.e. P150 and NP). In simulations, the top layers of parts were fabricated at the time 31305 s, when the laser scanned for the last time. It can be observed that in every deposited layer, the temperature reaches to the melting point temperature and subsequently drops from that temperature to the desired temperature (i.e. 150 °C for P150 and 22 °C for NP). It can be observed

that temperature decreases faster from 1370 °C to 22 °C for the NP process while it decreases from 1370 °C to 150 °C at the same time for P150 process. This trend shows that NP condition possesses a higher cooling rate than P150 condition.

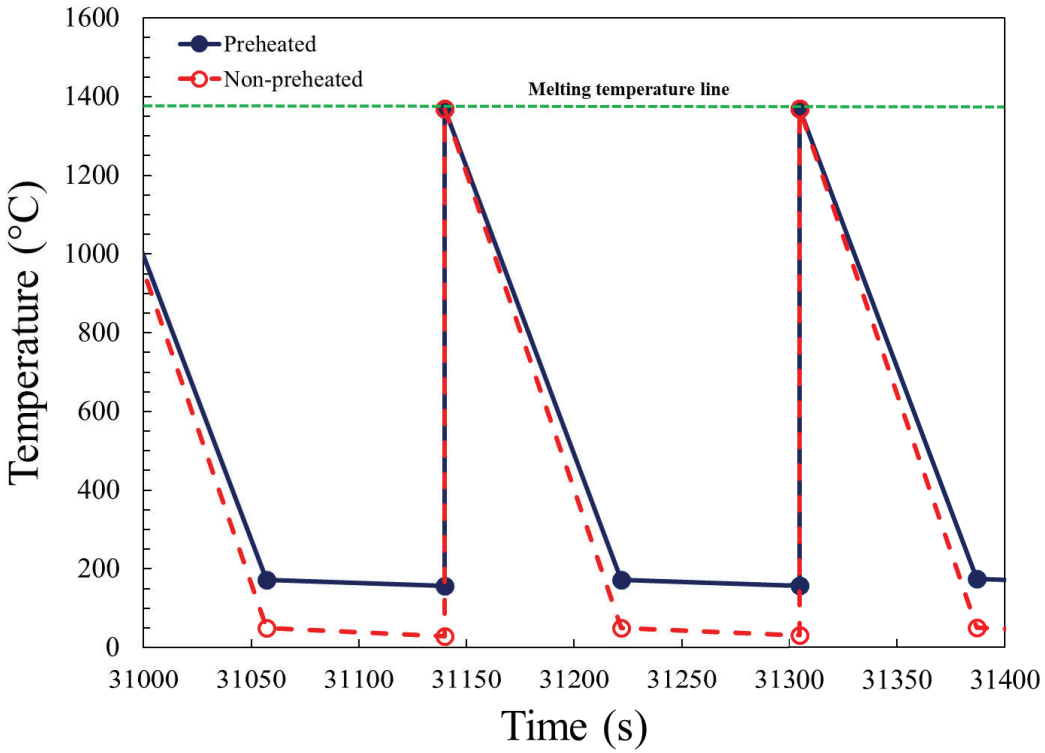

Figure 2. Temporal distribution of maximum temperature along the fabrication direction (z) for both P150 and NP conditions. Middle of the gauge section is scanned at time 31,305 s.

Masoomi et al. [14] reported that cooling rates are governed by the conduction, convection, and radiation within the heat affected zone (HAZ), i.e., the solid region in the vicinity of the melt pool, shielding gas, and the walls of the chamber, respectively. Since the effects of convection and radiation were neglected in this study, heat is dissipated by conduction in the HAZ. The conduction heat dissipation is dependent on the thermal gradient between two points, thereby, cooling rates are directly related to the temperature differences between these two points, which is in accordance to Newton law of cooling. Therefore, a higher temperature difference between two points can derive a higher cooling rate, which can be also observed in Figure 2. The cooling rate values were obtained from the simulation to be 1.43×10^6 °C/s for P150, and 1.65×10^6 °C/s for the NP condition. Some studies have shown that lower thermal gradients, and consequently, lower cooling rates, can result in melt pools with larger dimensions [15]. Therefore, larger melt pool dimensions including melt pool depth can be expected for the parts that are preheated.

Figure 3(a) and (b) show the melt pool dimensions for specimens fabricated without preheating (NP), and with preheating (P150) the build platform, respectively. The average width to depth ratios (i.e. W_{avg}/d_{avg}) of the melt pool is calculated for NP and P150 conditions to be 1.38 and 1.7, respectively. It can be seen that P150 condition has larger melt pools as compared to the NP one, which is consistent with the lower cooling rate calculated for the former condition (i.e.

P150). Moreover, melt pool size affects the porosity level due to the gas entrapment as argon cannot be dissolved in steels.

Comparing the microstructure obtained for P150 with NP condition, the cellular structure is seen in the former condition (shown with white arrows in Figure 3(b)). Based on the thermal simulation results shown in Figure 2, the decrease in the cooling rate by preheating the build platform is due to the lower temperature gradient induced between the layer melted and the previous fused layers. This results in not only grain structure modification but also the texture evolution [11]. Typically, formation of fine cellular-dendritic microstructure has been reported as the common microstructure produced in the AM process [16,17]. This is due to the heat dissipation toward the build platform. Formation of the cellular-dendritic structure has been also reported for LB-PBF 316L SS [18]. However, it has been shown that preheating the build platform results in more equiaxed grains [10]. Moreover, it has been reported that increasing the laser power (i.e. higher energy density) leads to the formation of equiaxed cellular structure in 316L SS [19]. Accordingly, the results obtained found the preheated platform condition to be consistent with the literature.

Figure 4(a) and (b) show the transverse plane in the gage section polished to characterize the porosity size and distribution for NP and P150 conditions, respectively. In addition, the porosity size and distribution histograms for each condition are plotted. Comparing the polished sections, the porosity level decreased for the specimens fabricated with preheating the build platform. The statistics results of porosity show that frequency of pores in P150 condition is higher in low size classes (i.e. [11-18] μm) as compared to the NP condition. Consequently, fewer large pores are seen for P150 condition. A larger and higher number of pores in NP condition is related to the relatively higher cooling rates in this condition as compared to P150. In fact, the entrapped gas does not get the chance to escape from melt pools due to rapid solidification, thereby, it results in more porosities.

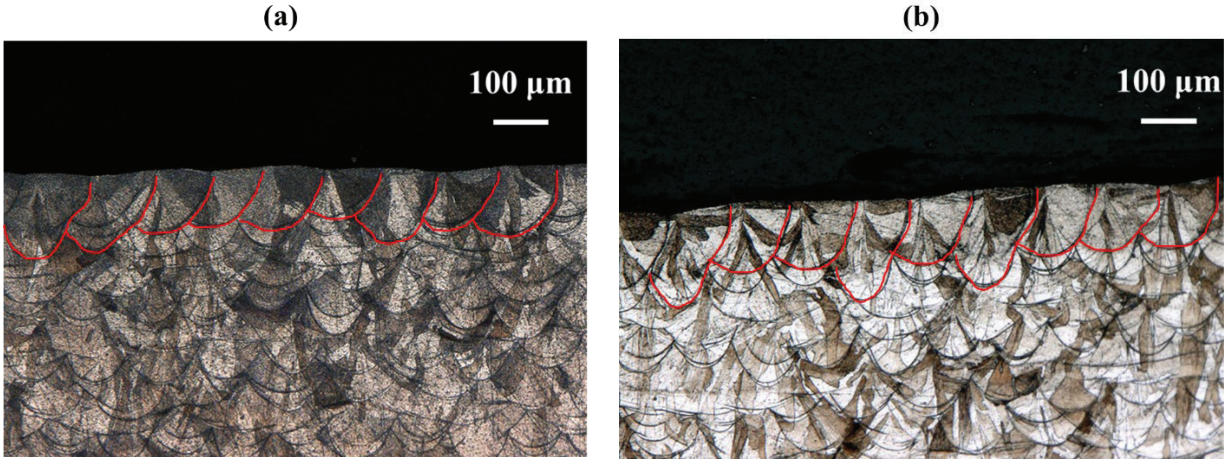

Figure 3. Melt pool characterization on the most top layer: (a) non-preheated, and (b) preheated build platform.

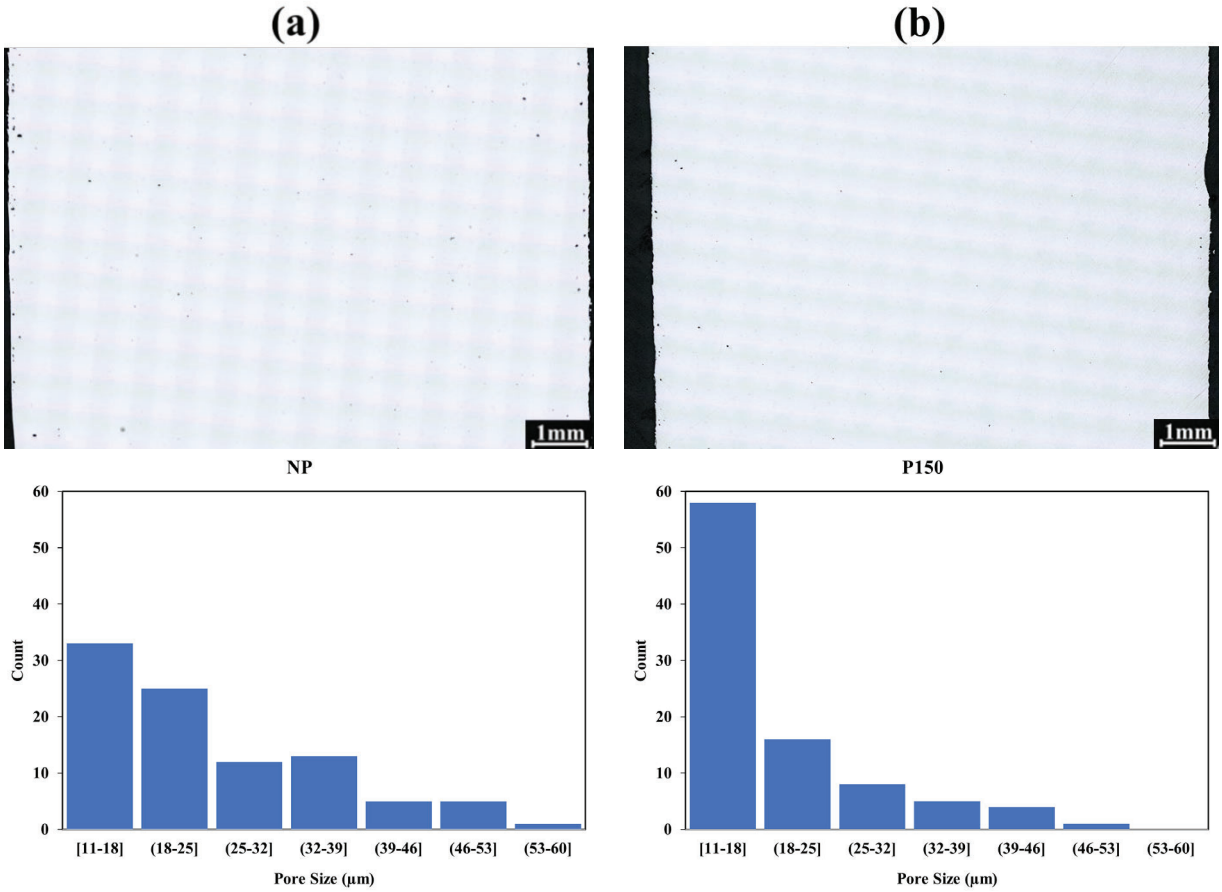

Figure 4. Porosity measurement results in the gage section: (a) polished section and porosity size distribution for non-preheated, and (b) polished section and porosity size distribution for preheated build platform conditions. Note the size classes for each condition.

Tensile properties

Monotonic tensile deformation behavior of specimens fabricated with and without preheating the build platform is shown in Figure 5. The strain-controlled mode portion of the tensile test is shown in Figure 5(a), and the stress-displacement curve from the beginning of the tests to the fracture is shown in Figure 5(b). Moreover, the tensile results are compared with [20] and wrought material [21–23], listed in Table 2. The ultimate tensile strength and elongation to failure (El%) of the present alloy increased as compared to those of additively manufactured and wrought counterparts. Interestingly, preheating the build plate increased the El% and yield strength (σ_y) of the material by approximately 14% and 4%, respectively. This is attributed to the microstructure and texture evolution. As seen in Figure 3(b) shown by white arrows, the cellular structure has been developed in the P150 condition. These cellular structures, either dendritic- or equiaxed-cellular structures, are made of high dislocation density as a result of the high cooling rate during fabrication [18]. However, in P150 condition, dislocation rearrangement and recovery may occur and lead into the equiaxed-cellular structure, as the previously fused layers are still at high temperature [24]. Accordingly, dislocation density is decreased, and the microstructure might be considered similar to the annealed condition. Therefore, the material is capable of

accommodating higher plastic deformation by generation of geometry necessary dislocations (GND) during straining the material [25].

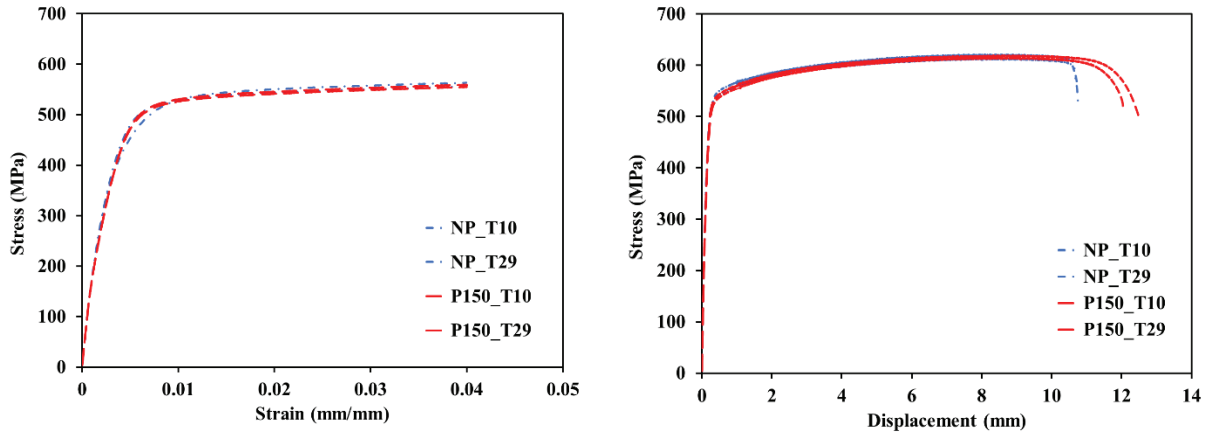

Figure 5. Tensile deformation behavior of LB-PBF 316L SS fabricated both in non-preheated and preheated build plate conditions: (a) stress-strain up to 0.045 strain, and (b) stress-displacement to fracture

Table 2. Monotonic tensile properties of 316L SS fabricated under argon shielding gas in both non-preheated and preheated build platform conditions.

Build platform conditions	σ_y (MPa)	σ_u (MPa)	El%
Non-preheated	448	617	72
Preheated	465	618	82
LB-PBF 316L [20]	485	594	58
Wrought [21][22,23]	255-310	535-623	30-40

Fractography

Figure 6 shows the fracture surfaces of tensile specimens for the non-preheated and preheated conditions. As seen, both fracture surfaces exhibited cup and cone type failure and consisted of fibrous and shear region. These fracture features are consistent with the tensile results obtained, showing ductile behavior of the material. As seen in Figure 6(a), NP specimen has larger fibrous region than that of P150 specimen, however, tensile results show lower ductility for the former condition. This is due to the lower structural integrity of NP condition resulted from higher porosity level as compared to P150 condition. Moreover, although dimples exist in both conditions (shown by red arrows), the specimens fabricated on the preheated build platform consist of deeper dimples (~ 25-27 μm) as compared to those of the ones fabricated on the non-preheated build platform (~ 15-21 μm). Deeper dimples are the sign of higher ductility in the material, which can be seen that the P150 specimens possess higher ductility than NP ones. Shallower dimples in NP condition can also be due to less structural integrity in this condition due to the presence of more

porosities and lack- of-fusion (LOF) defects as compared to the P150 condition (see Figure 4). Shrestha et al. [20] also showed various LOF defects in the fracture surfaces of LB-PBF 316L SS fabricated with non-preheated build platform condition.

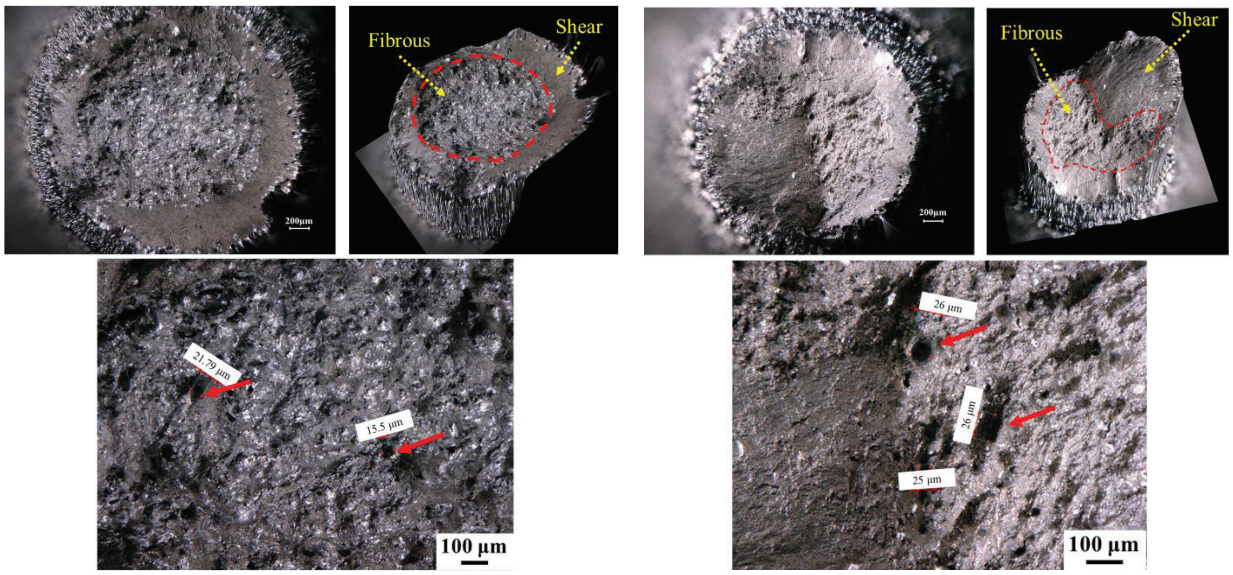

(a) (b)

Figure 6. Tensile fracture surfaces of LB-PBF 316L SS specimens: (a) non-preheated, and (b) preheated build platform conditions.

Conclusions and future study

The effect of preheating the build platform on the microstructure and mechanical properties of LB-PBF 316L SS was investigated. The following conclusions can be drawn based on the results:

1. The cooling rate of P150 condition was decreased as compared to that of the NP condition. This resulted into formation of equiaxed cellular structure.
2. Preheating the build platform to 150 °C increased the ductility of material by 14%. This is attributed to the more homogenized microstructure as well as cellular structure with geometry necessary dislocations (GNDs), thereby material accommodated more plastic strains during deformation.
3. The porosity size and distribution were decreased by preheating the build platform. The critical defect size for the NP condition was in the range of [32-39], while it was in the range of [17-24] for the P150 condition.
4. Tensile fracture surfaces of P150 specimens were found to have less fibrous region as compared to NP ones. However, due to the higher structural integrity of P150 (i.e. less porosity and lack of fusion defects) than NP specimens, ductility increased without any change in the material strength.

Due to the significant effect of preheating the build platform on reducing the porosity size and distribution, fatigue performance of the material assumed to be enhanced as compared to the condition without preheating the build platform. Therefore, in the next step of our study we are investigating the fatigue behavior of LB-PBF 316L SS fabricated in both preheated and non-preheated build platform conditions with as-built and machined surface conditions.

Acknowledgments

This material is based upon the work supported by the U.S. Naval Air Systems Command (NAVAIR).

References

[1] S.R. Daniewicz, N. Shamsaei, An introduction to the fatigue and fracture behavior of additive manufactured parts, Int. J. Fatigue. 94 (2017) 167. doi:10.1016/j.ijfatigue.2016.07.007.

[2] Y. Kok, X.P. Tan, P. Wang, M.L.S. Nai, N.H. Loh, E. Liu, S.B. Tor, Anisotropy and heterogeneity of microstructure and mechanical properties in metal additive manufacturing: A critical review, Mater. Des. 139 (2018) 565–586. doi:10.1016/j.matdes.2017.11.021.

[3] N. Shamsaei, A. Yadollahi, L. Bian, S.M. Thompson, An overview of Direct Laser Deposition for additive manufacturing; Part II: Mechanical behavior, process parameter optimization and control, Addit. Manuf. 8 (2015) 12–35. doi:10.1016/j.addma.2015.07.002.

[4] R. Shrestha, P.D. Nezhadfar, M. Masoomi, J. Simsiriwong, N. Pham, N. Shamsaei, Effects of Design Parameters on Thermal History and Mechanical Behavior of Additively Manufactured 17-4 PH Stainless Steel, in: 2018.

[5] A. Yadollahi, N. Shamsaei, S.M. Thompson, A. Elwany, L. Bian, Effects of building orientation and heat treatment on fatigue behavior of selective laser melted 17-4 PH stainless steel, Int. J. Fatigue. (2015). doi:10.1016/j.ijfatigue.2016.03.014.

[6] P.D. Nezhadfar, M. Masoomi, S.M. Thompson, N. Phan, N. shamsaei, Mechanical Properties of 17-4 PH Stainless Steel Additively Manufactured under Ar and N2 Shielding Gas, Solid Free. Fabr. Symp. – An Addit. Manuf. Conf. (2018) 1301–1310.

[7] H.G. Hengfeng Gu Deepankar Pal, Khalid Rafi, Thomas Starr, Brent Stucker, Influences of Energy Density on Porosity and Microstructure of Selective Laser Melted 174PH Stainless Steel, (2013).

[8] S.-H. Sun, T. Ishimoto, K. Hagihara, Y. Tsutsumi, T. Hanawa, T. Nakano, Excellent mechanical and corrosion properties of austenitic stainless steel with a unique crystallographic lamellar microstructure via selective laser melting, Scr. Mater. 159 (2019) 89–93. doi:10.1016/J.SCRIPTAMAT.2018.09.017.

[9] R. Mertens, B. Vrancken, N. Holmstock, Y. Kinds, J.-P. Kruth, J. Van Humbeeck, Influence of Powder Bed Preheating on Microstructure and Mechanical Properties of H13 Tool Steel SLM Parts, Phys. Procedia. 83 (2016) 882–890. doi:10.1016/J.PHPRO.2016.08.092.

[10] K. V Yang, Y. Shi, F. Palm, X. Wu, P. Rometsch, Columnar to equiaxed transition in Al-Mg(-Sc)-Zr alloys produced by selective laser melting, Scr. Mater. 145 (2018) 113–117. doi:10.1016/j.scriptamat.2017.10.021.

[11] W. Li, J. Liu, Y. Zhou, S. Wen, Q. Wei, C. Yan, Y. Shi, Effect of substrate preheating on the texture, phase and nanohardness of a Ti–45Al–2Cr–5Nb alloy processed by selective laser melting, Scr. Mater. 118 (2016) 13–18. doi:10.1016/J.SCRIPTAMAT.2016.02.022.

[12] S.L. Sing, J. An, W.Y. Yeong, F.E. Wiria, Laser and electron-beam powder-bed additive manufacturing of metallic implants: A review on processes, materials and designs, J. Orthop. Res. 34 (2016) 369–385. doi:10.1002/jor.23075.

[13] Y. Li, D. Gu, Parametric analysis of thermal behavior during selective laser melting additive manufacturing of aluminum alloy powder, Mater. Des. 63 (2014) 856–867. doi:10.1016/J.MATDES.2014.07.006.

[14] M. Masoomi, S.M. Thompson, N. Shamsaei, Laser powder bed fusion of Ti-6Al-4V parts:

Thermal modeling and mechanical implications, Int. J. Mach. Tools Manuf. 118–119 (2017) 73–90. doi:10.1016/J.IJMACHTOOLS.2017.04.007.
[15] Y. Li, D. Gu, Parametric analysis of thermal behavior during selective laser melting additive manufacturing of aluminum alloy powder, Mater. Des. 63 (2014) 856–867. doi:10.1016/J.MATDES.2014.07.006.
[16] O. Andreau, P. Peyre, J.D. Penot, I. Koutiri, C. Dupuy, E. Pessard, N. Saintier, Deterministic defect generation in selective laser melting: parametric optimization and control, Lasers Manuf. - WLT EV. (2017) 1–11.
[17] P.D. Nezhadfar, R. Shrestha, N. Phan, N. Shamsaei, Fatigue Behavior of Additively Manufactured 17-4 PH Stainless Steel: Synergistic Effects of Surface Roughness and Heat Treatment, Int. J. Fatigue. (2019).
[18] O. Andreau, I. Koutiri, P. Peyre, J.-D. Penot, N. Saintier, E. Pessard, T. De Terris, C. Dupuy, T. Baudin, Texture control of 316L parts by modulation of the melt pool morphology in selective laser melting, J. Mater. Process. Technol. 264 (2019) 21–31. doi:10.1016/J.JMATPROTEC.2018.08.049.
[19] J.D. Majumdar, A. Pinkerton, Z. Liu, I. Manna, L. Li, Microstructure characterisation and process optimization of laser assisted rapid fabrication of 316L stainless steel, Appl. Surf. Sci. 247 (2005) 320–327. doi:10.1016/J.APSUSC.2005.01.039.
[20] R. Shrestha, J. Simsiriwong, N. Shamsaei, Fatigue behavior of additive manufactured 316L stainless steel parts: Effects of layer orientation and surface roughness, Addit. Manuf. 28 (2019) 23–38. doi:10.1016/J.ADDMA.2019.04.011.
[21] B. Zhang, L. Dembinski, C. Coddet, The study of the laser parameters and environment variables effect on mechanical properties of high compact parts elaborated by selective laser melting 316L powder, Mater. Sci. Eng. A. 584 (2013) 21–31. doi:10.1016/J.MSEA.2013.06.055.
[22] M. Ziętala, T. Durejko, M. Polański, I. Kunce, T. Płociński, W. Zieliński, M. Łazińska, W. Stępniowski, T. Czujko, K.J. Kurzydłowski, Z. Bojar, The microstructure, mechanical properties and corrosion resistance of 316 L stainless steel fabricated using laser engineered net shaping, Mater. Sci. Eng. A. 677 (2016) 1–10. doi:10.1016/J.MSEA.2016.09.028.
[23] J. POLÁK, K. OBRTLÍK, M. HÁJEK, Cyclic plasticity in type 316L austenitic stainless steel, Fatigue Fract. Eng. Mater. Struct. 17 (1994) 773–782. doi:10.1111/j.1460-2695.1994.tb00808.x.
[24] F.J. Humphreys, M. Hatherly, Recrystallization and related annealing phenomena, Elsevier, 2004.
[25] K. Obrtlík, T. Kruml, J. Polák, Dislocation structures in 316L stainless steel cycled with plastic strain amplitudes over a wide interval, Mater. Sci. Eng. A. 187 (1994) 1–9. doi:10.1016/0921-5093(94)90325-5.